Electronic Supplementary Material (ESI) for Soft Matter.

Supplemental Information

Insight into the Nanostructure of Anisotropic Cellulose Aerogels upon Compression

Harald Rennhofer[§#*], Sven F. Plappert[†‡#], Helga C. Lichtenegger[§], Sigrid Bernstorff[⊥], Michael Fitzka[§], Jean-Marie Nedelec[‡], Falk W. Liebner[†]

[§] Institute of Physics and Material Sciences, University of Natural Resources and Life Sciences Vienna, Peter-Jordan-Straße 82, 1190 Vienna, Austria

[†]Division of Chemistry of Renewable Resources, University of Natural Resources and Life Sciences Vienna, Konrad-Lorenz-Straße 24, 3430 Tulln, Austria

[‡]Université Clermont Auvergne, CNRS, SIGMA Clermont, ICCF, F-63000 Clermont-Ferrand, France

[⊥]Elettra - Sincrotrone Trieste S.C.p.A., Strada Statale 14, 34149 Basovizza, Trieste, Italy

[#] Both authors contributed equally

Setup:

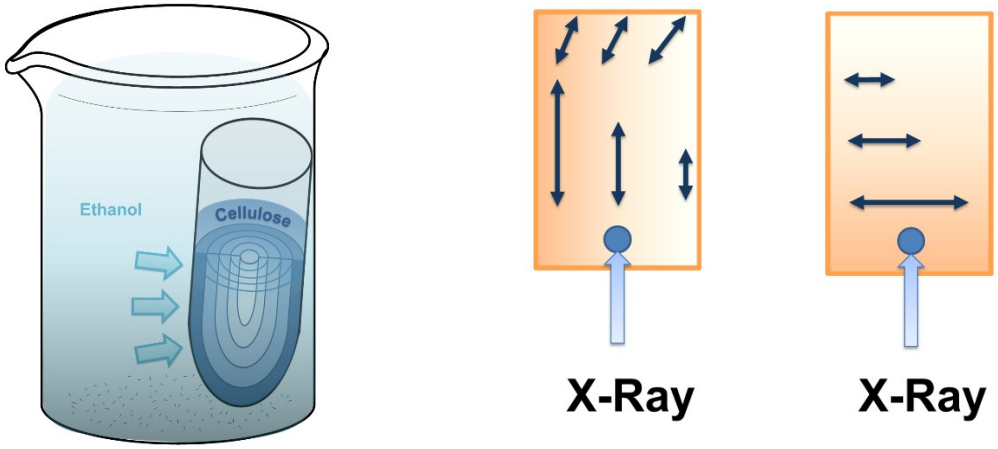

Figure S1: Experimental conditions. Left Panel - Gelation process: The mold is filled with dissolved cellulose and then submerged in the ethanol bath. The mold allows diffusion of ethanol into the cellulose solution and diffusion of TmGH[OAc] outwards into the bath, i.e. solvent and antisolvent are exchanged. Right Panel – Sample orientation in the X-ray beam: The beam hits the 12 mm high and 7.5 mm wide samples at the lower edge about in the middle. The blue circle is indicating where the X-ray beam hits the sample, which is compressed from above. The sample colour gradient and the blue double arrows indicate the degree of anisotropy in the sample.

Figure S1 right panel shows the positioning of the samples in the beam in detail, taking the inhomogeneity of the samples into account. For samples with structure parallel to the loading axis the degree or orientation decreases slightly from one side to the other, while it is constant throughout the height of the sample. They might feature slight curvature of the structure on the top part, due to the curvature of the sample mold (see left panel of Figure S1). For samples

with structure orthogonal to the loading axis the degree or orientation decreases slightly from top to bottom, while it is constant at one given height throughout the cross-section of the sample.

Uniformity of compression of the samples:

To monitor the uniformity of compression of the samples throughout the full sample height, during the course of the experiment, the expected change in the X-ray transmission dependent on the compression strain was calculated and experimental data for the transmission are compared to the calculated values. If *D* is the effective thickness (*i.e.* path length of the X-ray beam through absorbing cellulose) of a sample and μ an absorption coefficient the transmission T can be expressed by: $T = exp[-\mu D]$. For the aerogels with the high porosity, *D* is proportional to the density ρ of the bulk material, *i.e.* $D \sim \rho$. Since compression of the aerogel does not change the external dimensions, but lets the bulk sample collapse in itself by densification of the cellulose rods the density ρ can be expressed as function of the initial density ρ_0 and compressive strain *c* by:

$$\rho(c) = \rho_0 \frac{1}{1-c}$$

Thus T can be rewritten as function of the compressive strain as:

$$T(c) = e^{-\mu\rho(c)}$$

Given a value for an initial transmission T_0 measured for the sample with 34 mg / cm^{-1} (orthogonal orientation) before compression a nominal value for $\mu \cdot \rho_0$ can be found. With this information nominal values for T(c) have been calculated to give a nominal curve for the transmission.

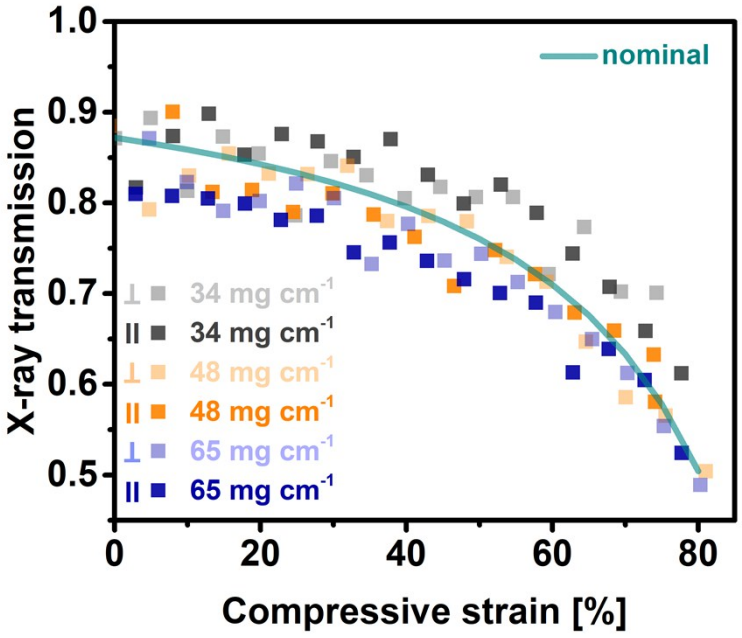

Figure S2: X-ray transmission measured during the *in-situ* experiments. The measurement data are depicted as symbols, while the expected change T(c) is depicted as line.

In Figure S2 it can be seen that all transmissions measured near the base of the aerogel samples change in a similar way as the calculation predicts. This behaviour shows that the samples are compressed homogenous throughout the full sample volume, *i.e.* that the change of the network monitored near the base of the sample is representative for the change in the full sample volume. Thus the measurement position at the lower end of the sample is valid to monitor the changes of the sample during compression since compression proceeds homogeneously over the entire height of the sample.

Details about the SAXS evaluation:

The aerogel network shows the same main fibril radius of about 3.1 nm throughout the compression experiment of a (48 mg cm^{-3}) sample. The fibril radius is around 3 nm for all samples and shows similar trends.

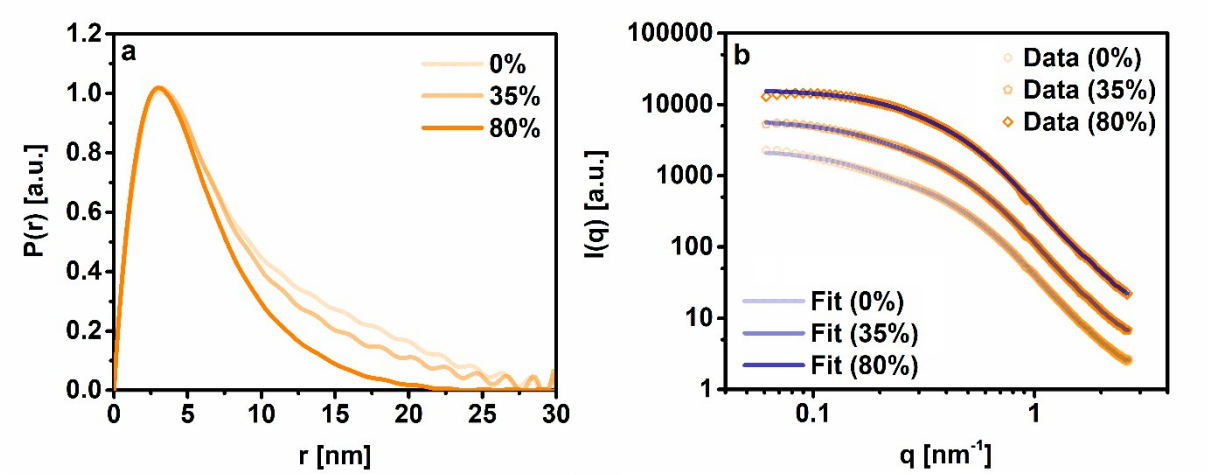

Figure S3: Typical fit of the scattering data with GNOM program: Distance distribution functions (left panel) and corresponding scattering data with the fit curves in I(q) representation (right panel). Scattering curves recorded at 0%, 35% and 80% compression from a sample with bulk density of (48 mg cm^{-3}).

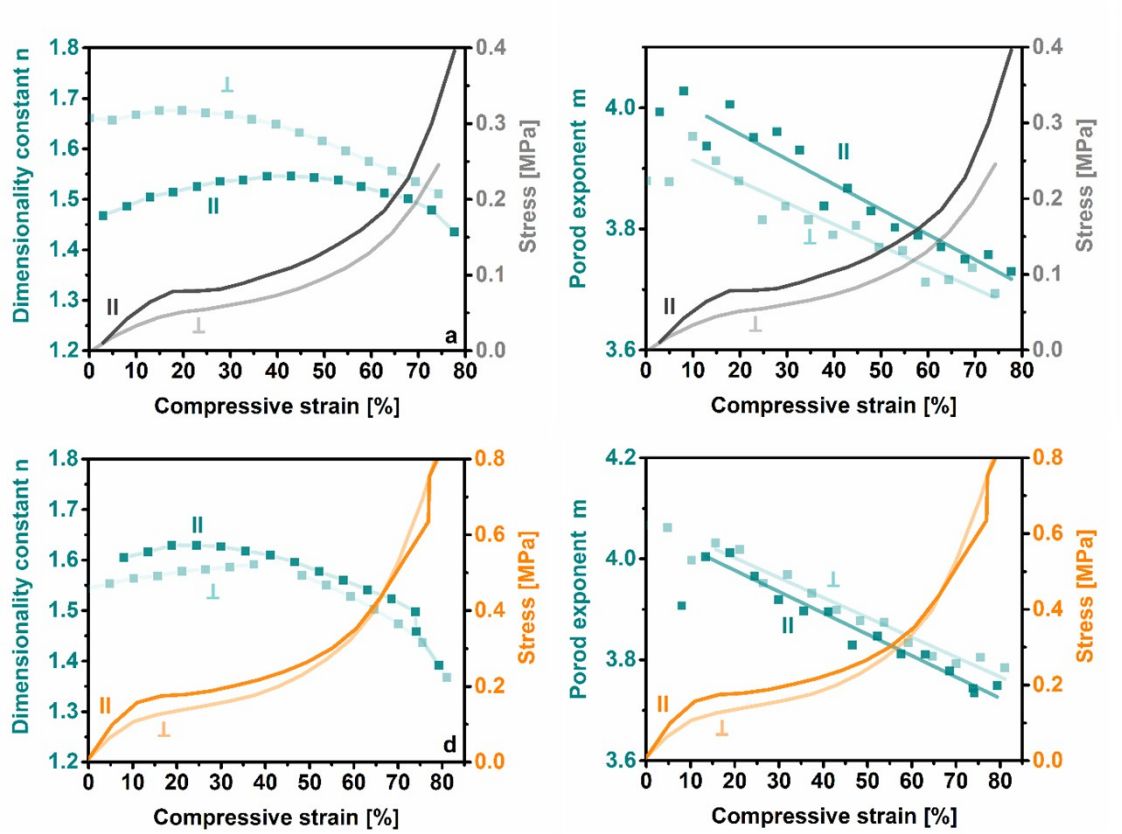

Figure S4: Additional data of the samples with 34 mg cm^{-3} (upper line) and with 48 mg cm^{-3} (lower line). The diagrams show the dimensionality parameter *n*, evaluated in the low q regime, the Porod exponent *m* and the evaluated for high-q regime together with the stress-strain curves.

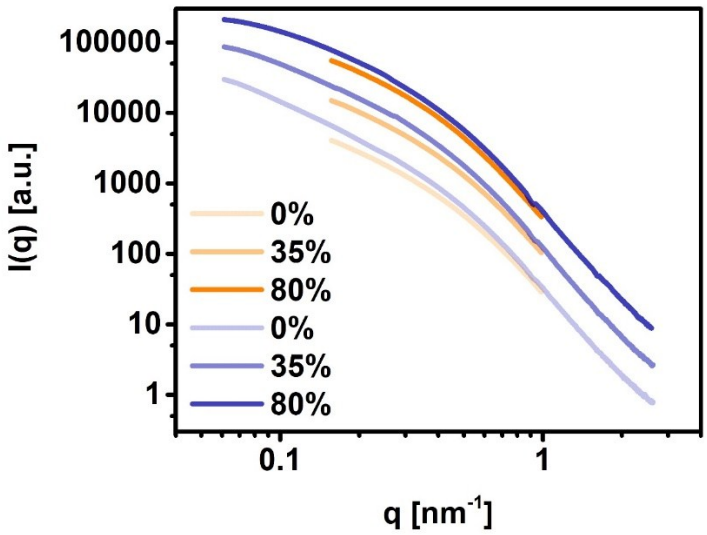

Figure S5: Comparison of scattering curves I(qx) and I(qy) evaluation from a sample with bulk density of (48 mg cm^{-3}) at 0%, 35% and 80% compressive strain. I(qx) are depicted orange and are evaluated in a much smaller q-range, I(qy) curves are blue and are evaluated in the full accessible q-range.

The sample material is inhomogeneous, but the experimental setup allows to access the full q-range needed for detailed evaluation only in the I(qy) direction, which is parallel to the loading axis and thus probing mainly oriented structures orthogonal to the loading axis. To better understand the changes in the sample an evaluation in I(qx) direction was performed.

I(qx) was obtained by an integration of the scattering curves in the azimuthal range from 150 to 210 degrees and limited q-range 0.16-0.1 nm^{-1}, I(qy) was obtained by an integration of the scattering curves in the azimuthal range from 240 to 300 degrees and full q-range 0.05-0.3 nm^{-1}.

Figure S5 shows the small discrepancy between I(qx) and I(qy) data. I(qx) shows a different curvature in the low-q region. During compression I(qx) stays the same and does not show changes, while I(qy) undergoes the changes described in the main article.

Evaluation of the Orientation Parameter S:

To be comparable to our previous work[1] the evaluation of the orientation parameter S was applied in a similar way. The scattering pattern of the partly oriented cellulose fibrils shows a typical oriented signal. In this case the azimuthal intensity distribution $I(\chi)$ features two Gaussian shaped peaks, 180 degrees apart, i.e. intensity originating from oriented fibrils on top of a constant background, , i.e. intensity originating from non-oriented fibrils or junctions.

Due to the actual position and orientation of the scattering pattern on the detector only part of these two Gaussian peaks, namely the peak between 40 and 120 degrees can be determined clearly, see Fig 6 in the main article. Thus only this peak was taken into account for the evaluation of the parameter S. This first Gaussian shaped peak of the scattering curve $I(\chi)$ was approximated by a curve fit with a Gaussian curve. From the obtained parameters (Intensity, width) the area A of the full peak was calculated and the background level from the fit was used in order to calculated the area A_c below the full Gaussian curve. Given these two parameters S was calculated: With A the area of the Gaussian peak and A_c the area of the constant background, S was defined as

$$S = A / (A + A_c).$$

S would equal one for mainly oriented fibrils, only featuring intensity in the Gaussian peak and zero for non-oriented fibrils, featuring a constant intensity distribution $I(\chi)$.

Effect of compression on pore structure:

The effect of compression on the pore structure of a cylindrical aerogels sample was assessed by nitrogen sorption experiments at 77K. An uncompressed sample as well as a sample uniaxially compressed to 40% of its initial height were measured. The initial bulk density of the aerogel samples was 48 mg cm^{-3} which was increased to about 240 mg cm^{-3} in case of the compressed sample. The aerogels were degassed at 50 °C for 20 hours (VacPrep 061, Micromeritics) prior to the measurement. Nitrogen adsorption and desorption isotherms were recorded on a TriStar II *PLUS* (Micromeritics, France). The pore size distributions was calculated by the Barrett–Joyner–Halenda (BJH) method[2] from the desorption branch of the isotherm.

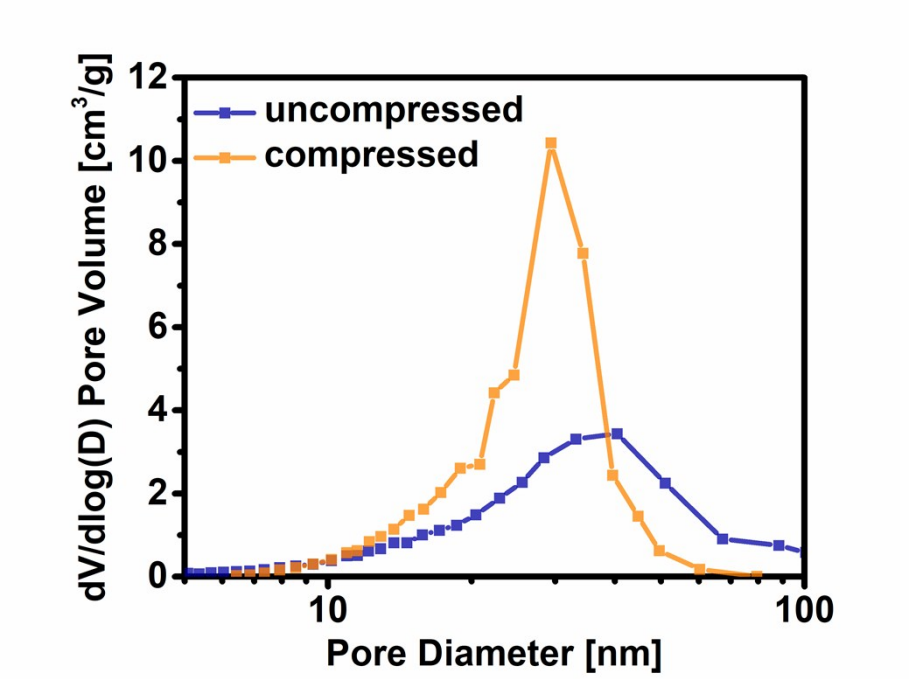

***Figure* S6:** Pore size distributions calculated from N_2 desorption isotherms via the BJH method for an uncompressed anisotropic aerogel and an anisotropic aerogel sample uniaxially compressed to 40% of its initial height

The uniaxial compression of the anisotropic cellulose II aerogels clearly impacts the materials pores size distribution shifting it towards smaller pore sizes as evident from the N_2 sorption experiments (*cf.* Figure S6). Additionally, the volume of pores in the range of 2-100 nm is increased from about 1,78 to 2,44 $cm^3\ g^{-1}$. Moreover only a minor decrease of the samples specific surface area was detected from the N_2 adsorption isotherm evaluated by the Brunauer–Emmett–Teller (BET) equation[3]. These results[4] are in line with previous studies on uniaxial densification of anisotropic aerogels constructed from cellulose I nanofibers. The effectuated pore size harmonization can be hence be applied to tailor one of the most important structural properties of the aerogels *i.e.* their pore size. Subsequently these results emphasize the applicability of uniaxial densification as an impactful tool in porous soft material design.

References

1. S. F. Plappert, J. M. Nedelec, H. Rennhofer, H. C. Lichtenegger, S. Bernstorff and F. W. Liebner, *Biomacromolecules*, 2018, **19**, 4411-4422.
2. E. P. Barrett, L. G. Joyner and P. P. Halenda, *J. Am. Chem. Soc.*, 1951, **73**, 373-380.
3. S. Brunauer, P. H. Emmett and E. Teller, *J. Am. Chem. Soc.*, 1938, **60**, 309-319.
4. S. F. Plappert, J.-M. Nedelec, H. Rennhofer, H. C. Lichtenegger and F. W. Liebner, *Chem. Mater.*, 2017, **29**, 6630-6641.